

Global and Local Mechanical Properties of Autogenously Laser Welded Ti-6Al-4V

XINJIN CAO, ABU SYED H. KABIR, PRITI WANJARA, JAVAD GHOLIPOUR, ANAND BIRUR, JONATHAN CUDDY, and MAMOUN MEDRAJ

Ti-6Al-4V sheets, 3.2-mm in thickness, were butt welded using a continuous wave 4 kW Nd:YAG laser welding system. The effect of two main process parameters, laser power and welding speed, on the joint integrity was characterized in terms of the joint geometry, defects, microstructure, hardness, and tensile properties. In particular, a digital image correlation technique was used to determine the local tensile properties of the welds. It was determined that a wide range of heat inputs can be used to fully penetrate the Ti-6Al-4V butt joints during laser welding. At high laser power levels, however, significant defects such as underfill and porosity, can occur and cause marked degradation in the joint integrity and performance. At low welding speeds, however, significant porosity occurs due to its growth and the potential collapse of instable keyholes. Intermediate to relatively high levels of heat input allow maximization of the joint integrity and performance by limiting the underfill and porosity defects. In considering the effect of the two main defects on the joint integrity, the underfill defect was found to be more damaging to the mechanical performance of the weldment than the porosity. Specifically, it was determined that the maximum tolerable underfill depth for Ti-6Al-4V is approximately 6 pct of the workpiece thickness, which is slightly stricter than the value of 7 pct specified in AWS D17.1 for fusion welding in aerospace applications. Hence, employing optimized laser process parameters allows the underfill depth to be maintained within the tolerable limit (6 pct), which in turn prevents degradation in both the weld strength and ductility. To this end, the ability to maintain weld ductility in Ti-6Al-4V by means of applying a high energy density laser welding process presents a significant advantage over conventional arc welding for the assembly of aerospace components.

DOI: 10.1007/s11661-013-2106-z

© The Minerals, Metals & Materials Society and ASM International 2013

I. INTRODUCTION

TITANIUM alloys have been widely used in the aerospace industry due to their high specific strength and excellent corrosion resistance.^[1] As the workhorse grade of

the titanium industry, Ti-6Al-4V is an alpha–beta alloy that is heat treatable and has a maximum service temperature of 673 K (400 °C).^[2] However, Ti-6Al-4V is difficult to weld due to the inherent high reactivity of titanium with atmospheric gases at elevated temperatures, especially in the liquid state.^[3] Hence, expanding the application of Ti-6Al-4V requires an effective and cost-efficient joining technology.

Ti-6Al-4V has been fusion welded using conventional arc and electron beam welding technologies, and more recently with laser welding, of which the latter offers considerable promise due to an interesting combination of some characteristics, including manufacturing flexibility (*e.g.* non-vacuum, local shielding gas protection), high energy density, low heat input, high welding speed, narrow size of the fusion and heat affected zones (HAZ), and low weld distortion.^[4] Similar to the electron beam, the laser beam is a line-shaped heating source through the joint thickness, as compared to a point heating source for conventional arc welding,^[5] but without the disadvantage of a confined environment for vacuum protection. Laser welding also produces a fusion zone (FZ) microstructure that comprises of small prior- β grains (due to the rapid solidification at low heat input) that are similar in size to that observed in electron beam weldments, but considerably finer than those in conventional arc welds.^[6] In addition, laser welding has the flexibility for welding autogenously or with filler wire

XINJIN CAO, Senior Research Officer, is with the Structures, Materials and Manufacturing Laboratory, National Research Council Canada - Aerospace, 5145 Decelles Avenue, Montreal, QC H3T 2B2, Canada, and also Adjunct Professor, with the Department of Mechanical and Industrial Engineering, Concordia University, 1455 De Maisonneuve Blvd. West, Montreal, QC H3G 1M8, Canada. Contact e-mail: xinjin.cao@cnrc-nrc.gc.ca ABU SYED H. KABIR, formerly Master Graduate Student, with the Structures, Materials and Manufacturing Laboratory, National Research Council Canada - Aerospace, also with the Department of Mechanical and Industrial Engineering, Concordia University, is now Ph.D. Candidate with the McGill University, Montreal, QC H3A 0C5, Canada. PRITI WANJARA, Team Leader, and JAVAD GHOLIPOUR, Senior Research Officer, are with the Structures, Materials and Manufacturing Laboratory, National Research Council Canada - Aerospace. ANAND BIRUR and JONATHAN CUDDY, Senior Engineers, are with the StandardAero Limited, 33 Allen Dyne Road, Winnipeg, MB R3H 1A1, Canada. MAMOUN MEDRAJ, Professor, is with the Department of Mechanical and Industrial Engineering, Concordia University.

The following statement pertains only to authors X. Cao, A.S.H. Kabir, and P. Wanjara: Published with permission of the Crown in Right of Canada, i.e., the Government of Canada.

Manuscript submitted June 13, 2013.

addition.^[7] Effective shielding gas protection remains an important criterion for laser welding, but the lower energy and shorter welding time as compared to arc welding mitigate contamination of the molten weld pool from atmospheric elements, allowing improved ductility for the joints assembled with the former process.^[6]

To this end, as part of a larger program on the advanced manufacturing of aerospace materials at the National Research Council of Canada (NRC) the weldability of Ti-6Al-4V was investigated using a continuous wave (CW) 4 kW Nd:YAG laser system, the findings of which were reported previously in References 8 through 11. Of importance to the understanding of the joint integrity is characterization of the mechanical response of the weldment. Although the global or overall mechanical properties provide useful information for the welded assembly, the constitutive data for the different microstructural zones that comprise the “composite” structure of the weldment, *i.e.*, base metal (BM), HAZ and FZ, is important for evaluating whether the local mechanical response can meet the stress requirements in the service environment. To date, the local mechanical properties of friction stir welded aluminum alloys^[12,13] and laser welded 304L stainless steel^[14] have been investigated using an optical, full-field displacement measurement or digital image correlation (DIC) technique. Recently, the present authors have also evaluated the local mechanical properties of laser welded Ti-6Al-4V using DIC.^[8,11] In this work, the optimal parametric window for the laser welding process was established through evaluating the global and local mechanical properties and response of the Ti-6Al-4V weldments to have a better insight on the processing-structure-property interrelationship.

II. EXPERIMENTAL PROCEDURE

The sheet material used in this study was mill-annealed Ti-6Al-4V (Grade 5 titanium) with a nominal thickness of 3.2 mm. The samples were machined and had dimensions of 102 mm in length \times 63 mm in width. All welds were butt joints with no intentional gap and were welded along the sample length, which was perpendicular to the rolling direction. The faying and joining surfaces of all the samples were brushed and then cleaned with ethanol to remove any surface oxides and contaminants prior to clamping and welding. The welding equipment used was a 4 kW CW solid-state Nd:YAG laser system equipped with an ABB robot and a magnetic holding fixture. A collimation lens of 200 mm, a focal lens of 150 mm and a fiber diameter of 0.6 mm were employed to produce a focal spot diameter of about 0.45 mm. The top surface of the workpiece was shielded using high purity argon gas at a flow rate of 23.6 L/min (50 cfh), while the bottom surface and the trail on the top surface were shielded using a mixture of argon and helium (50 to 50 in vol pct) gases at a total flow rate of 66.1 L/min (140 cfh). The laser beam was focused at 1 mm under the top surface of the workpiece. Table I gives the laser welding process parameters (laser power, welding speed, heat input, and

power density) used in this study. The experiments were designed in a way to have a specific heat input using different combinations of the two main parameters (laser power and welding speed). It is noteworthy that the upper limit of the welding speed at a given laser power is bound by the presence of a lack-of-penetration (LOP) defect.

Three specimens were taken from the stable middle region of each joint for metallographic examination and microhardness evaluation. The specimens were then mounted, ground, polished, and etched by immersion in Kroll's reagent (1 to 3 mL HF + 2 to 6 mL HNO₃ + 100 ml H₂O) for 6 to 10 seconds. Microstructural examination was carried out using an inverted optical light microscope (Olympus GX71) equipped with AnalySIS Five digital image analysis software that allowed quantitative measurements of the defect size and fraction. Vickers micro-indentation hardness was measured at a load of 500 g, a dwell period of 15 seconds and, in accordance with ASTM E384-05, an indent interval of 0.2 mm^[11] using a Struers Duramin A-300 machine.

Four tensile coupons having a standard sub-size geometry of 25 mm in gauge length, 6 mm in width, and 3.2 mm in thickness were machined in accordance to ASTM E8M-04.^[15] All the tensile coupons were tested at room temperature and a constant crosshead rate of 2 mm/min using a 250 kN MTS testing frame equipped with a laser video extensometer. To evaluate the local tensile behavior for selected process conditions, an ARAMIS DIC system (GOM), as described in Reference 11, was also utilized during tensile testing. It is noteworthy that before executing the tensile tests, the front side of each coupon was painted with a high-contrast random pattern of black speckles on a white background, while on the back side two pieces of laser tape were attached to mark the gauge length for the laser extensometer during testing. To determine the local tensile properties, an iso-stress condition (*e.g.*, the same global tensile stress at all locations in the gauge length) was assumed for the analysis of tensile results as widely used for different alloys.^[12,13,16] The local strain data were then extracted from the DIC system for regions of interest within the gauge length and plotted against the corresponding global stress data to generate the local stress-strain response. Once the stress-strain diagram for a given location was generated, the corresponding local tensile properties, including the yield stress and plastic strain at fracture were determined.

III. RESULTS AND DISCUSSION

A. Weld Bead Geometry

Figure 1 shows the transverse sections of all the joints obtained using different laser process conditions with the objective of achieving full penetration across the joint thickness of 3.2 mm. The upper limit of the welding speed at a given laser power is determined by the presence of LOP defects. For example, at a laser power of 3 kW, the maximum welding speed is 3.38 m/min, since a LOP defect was observed at 4.5 m/min

Table I. Laser Welding Parameters Used in This Study and Tensile Failure Locations

#	Laser Power (kW)	Welding Speed (m/min)	Heat Input (J/mm)	Power Density (MW/cm ²)	Location of Tensile Failure
1	2.0	0.75	160	1.06	4 in BM
2	2.0	1.13	106	1.06	4 in BM
3	2.0	1.5	80	1.06	4 in BM
4	3.0	1.13	160	1.60	4 in BM
5	3.0	1.69	106	1.60	4 in BM
6	3.0	2.25	80	1.60	4 in BM
7	3.0	3.38	53	1.60	4 in BM
8*	3.0	4.5	40	1.60	4 in BM
9	4.0	3.0	80	2.13	4 in HAZ
10	4.0	4.5	53	2.13	4 in FZ
11	4.0	6.0	40	2.13	4 in FZ
12	4.0	7.5	32	2.13	2 in FZ, 2 in HAZ

*The joint was welded from both sides due to the lack of penetration after single-side welding.

(other welds with LOP defects obtained at 2 and 4 kW and their respective higher welding speeds are not shown here). It is noteworthy that this weld (3 kW, 4.5 m/min) was then welded again from the opposite side using the same processing parameters for full penetration; all results related to this joint are taken from the single-sided weld with a LOP except for the global and local tensile properties that were obtained from the double-sided weld.

With increasing laser power, the range of welding speeds that permitted full penetration increased. For example, at laser powers of 2, 3, and 4 kW, fully penetrated welds were obtained at welding speeds of approximately 0.75 to 1.50 m/min, 1.13 to 3.38 m/min, and 3.0 to 7.5 m/min, respectively. Therefore, a wider process window can be obtained at a higher laser power. Furthermore, it was determined that at a higher laser power, a lower heat input is needed for full penetration. For instance, the minimum heat inputs for full penetration with a single welding pass are about 80 J/mm at a laser power of 2 kW, 53 J/mm at 3 kW, and 32 J/mm at 4 kW. Therefore, a higher laser power can reduce the minimum heat input required for full penetration across a specific thickness.

Although a range of process conditions can achieve full penetration across the joint thickness, the weld bead geometry can vary considerably even when a similar heat input is used. For instance, at a heat input of 80 J/mm, full penetration across the joints was obtained for three different laser power and welding speed combinations, *i.e.*, at low (2 kW and 1.50 m/min), medium (3 kW and 2.25 m/min), and high (4 kW and 3.0 m/min) levels. However, as revealed in Figure 1, the intermediate process condition (3 kW, 2.25 m/min) results in a relatively better weld bead geometry and weld integrity, as remarked from the extent of the underfill depth and the porosity level (as discussed in detail in the next section) in the welds assembled at 4 and 2 kW, respectively. As apparent from Figure 1, with increasing heat input (or decreasing welding speed at a given laser power), both the FZ and HAZ sizes increase. Also with increasing heat input, the weld bead geometry evolves from a V-shape to an hourglass morphology and then to a wide near-rectangular profile, which reflects

the evolution in welding mode from keyhole to “near-conduction” that imparts a marked increase in the heat input and thus renders a large weld bead profile.

B. Weld Defects

As shown in Figures 1 and 2, the porosity in the Ti-6Al-4V laser welds was located near the FZ/HAZ interface and/or near the root of FZ at the weld centerline. Some scattered pores were also apparent in random regions, mostly probably due to the turbulent flow of the molten metal in liquid pool during laser welding. Figure 3 shows the percent porosity area in the FZ for the welds assembled at different laser powers and welding speeds. In general, the porosity area decreased with increasing welding speed. Particularly, the lowest porosity level occurred in the welds assembled at an intermediary laser power of 3 kW, with the exception of the joint with a LOP. At both low (2 kW) and high (4 kW) laser powers, the porosity area was greater than that at the intermediary power of 3 kW. In fact, the lowest laser power (2 kW) resulted in the maximum porosity area.

The nature and origin of the porosity have been documented and detailed in an earlier publication.^[17] It is generally believed that the porosity is mainly caused by the collapse of the keyhole and trapped gas bubbles in the molten material that may originate from shielding gas and surface contaminants such as oil and grease as well as existing porosity.^[4,17] Dawes^[18] reported that in closely fitted butt joints, the porosity fraction is lower in the fully penetrated joints than those with LOP defects. This supports the high porosity area measured in the weld assembled at 3 kW and 4.5 m/min that had a LOP (Figure 1); in closely fitted butt welds, when LOP occurs, the escape of the gas porosity before solidification is accessible only by means of the top surface. In contrast, for a fully penetrated weld, access to the top and bottom surfaces allows the bubbles to escape more effectively.^[18]

The spherical shape of most of the pores indicates gas type porosity, which could have originated from contamination (moisture, grease, oil, and dirt) on the material surface and their reactions with the liquid

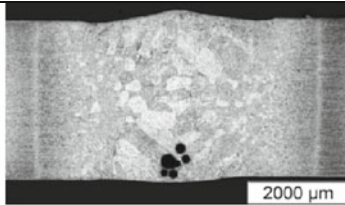
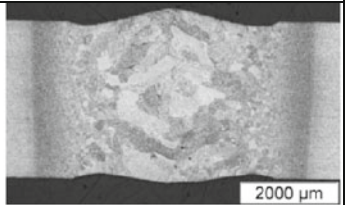
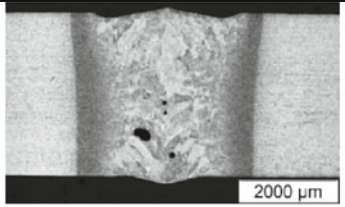
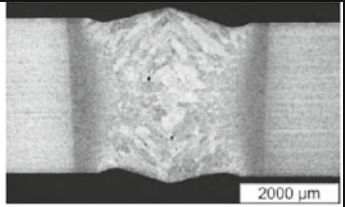
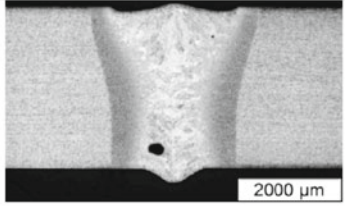
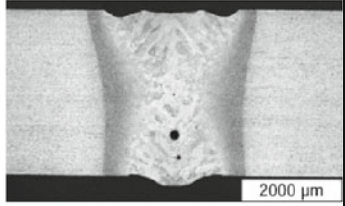
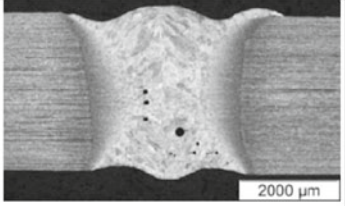
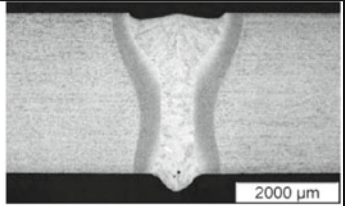
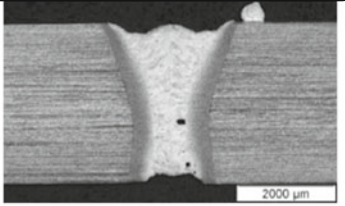
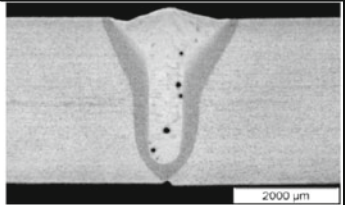
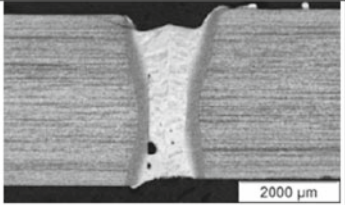
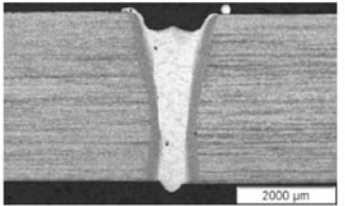
Heat input	2 kW	3 kW	4 kW
160 J/mm	 0.75 m/min	 1.13 m/min	
106 J/mm	 1.13 m/min	 1.69 m/min	
80 J/mm	 1.50 m/min	 2.25 m/min	 3.0 m/min
53 J/mm		 3.38 m/min	 4.5 m/min
40 J/mm		 4.5 m/min	 6 m/min
32 J/mm			 7.5 m/min

Fig. 1—Images of transverse weld sections obtained at various heat inputs.

metal.^[19,20] Hydrogen, adsorbed in the molten weld pool that cannot escape before solidification, is considered to be mainly responsible for the formation of gas pores in titanium alloys,^[20] particularly because the solubility of hydrogen increases with decreasing temperature in liquid titanium.^[21] The molten metal near the immediate vicinity of the keyhole has the highest temperature

(evaporation point) and it decreases progressively to the melting point at the fusion boundary; the solubility of hydrogen is thus more supersaturated at the weld center and tends to diffuse towards the fusion boundary, which explains the presence of hydrogen porosity at the FZ/HAZ interface. Also as liquid titanium has a higher solubility for hydrogen than solid titanium at the

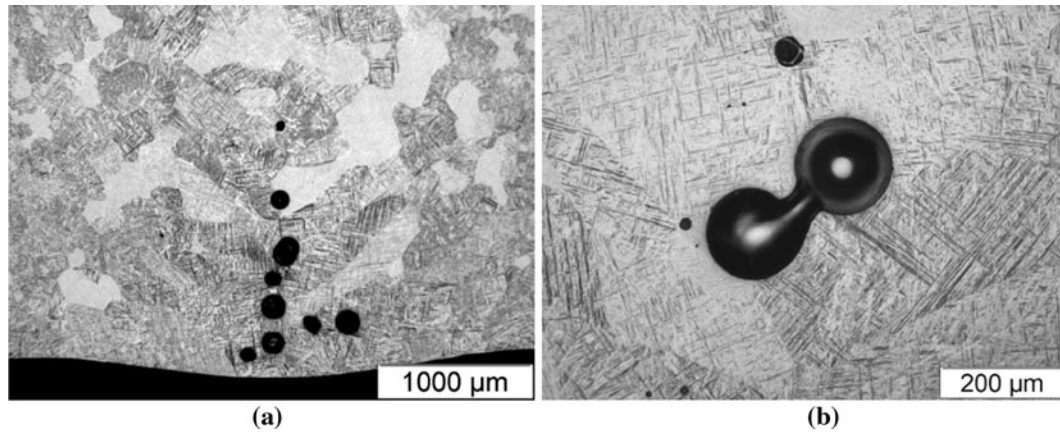


Fig. 2—Typical porosity or pore clusters obtained at a low laser power of 2 kW and welding speeds of (a) 0.75 m/min and (b) 1.13 m/min.

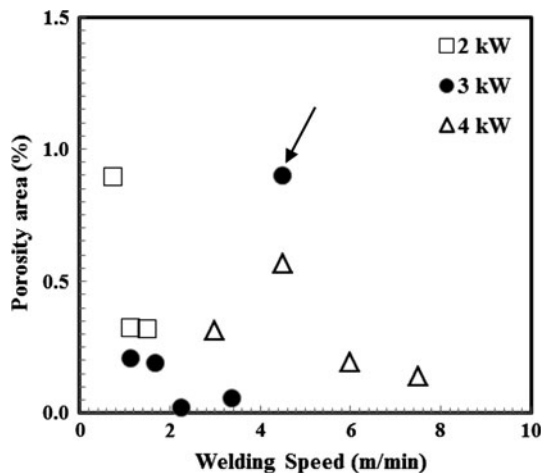


Fig. 3—Effect of laser power and welding speed on the porosity area (the arrow identifies the weld with a LOP that was then welded from both sides).

melting temperature,^[22] the centerline region of the weld pool is usually enriched in hydrogen; hydrogen gas can thus accumulate at the weld centerline, which is the last part of liquid/solid interface to solidify. Without an effective means for escape, due to the low temperatures at this late stage of solidification, the accumulated hydrogen gas is entrapped and leads to the higher amount of porosity at the centerline.^[23] It is noteworthy that though the centerline porosity is formed due to the evolution of hydrogen at the liquid/solid interface, the porosity in the root area can also be related to the instability of the keyhole.^[24]

The evolved hydrogen can form porosity by nucleation or direct diffusion into discontinuities or existing pores. Then these pores can grow and coalesce.^[22,25] At a low welding speed, the weld pool remains in the liquid state for a longer time, and thus the gas porosity can effectively grow. As a consequence, the porosity area would tend to decrease with increasing welding speed for a given laser power, which validates the observations in the present work (Figure 3). Specifically, both larger pores and higher porosity areas were apparent at higher

heat inputs due to the longer time available for the growth and coalescence of the voids. It was remarked that the porosity area was significantly greater for the 2 kW laser power conditions, particularly at the lowest welding speed of 0.75 m/min. These pores are mainly located in the lower part of the FZ (near weld root), as indicated in Figure 1. This is probably due to the relatively slow cooling rate associated with this lowest welding speed and the potential instability of the keyhole under such conditions. In particular, keyhole stability can only be achieved at high welding speeds^[26] and, for laser welding of Ti-6Al-4V with filler wire addition, the formation of significant porosity due to an unstable keyhole was reported at welding speeds less than 1 m/min.^[17] In spite of the high welding speeds for the 4 kW laser power conditions, high porosity area values were also observed, as shown in Figures 1 and 3. The use of a high laser power can slightly decrease the cooling rate and thus favor the growth of gas porosity, but the formation of evaporative porosity, caused by the high power density, is probably the main reason for the high porosity area as observed in this case.^[17] Hence, a reasonable combination of welding speed with an intermediate laser power (3 kW) can render minimized porosity, as illustrated in Figure 3. Though the existence of the porosity in the Ti-6Al-4V laser welds can reduce the load-bearing area and the mechanical properties of the joints, the total percent porosity was typically less than 1 pct of the FZ area (Figure 3). Hence, the characteristics of the underfill defect, that appears more prevalent in the images of the weld beads (Figure 1), may be more critical to the mechanical performance.

As shown in Figure 1, the underfill defects appear in all the Ti-6Al-4V laser welds, especially on the top surface and, at low welding speeds on the root surface also. Figure 4 illustrates the effect of the welding speed and power density on the underfill depth and area. According to AWS D17.1,^[27] the specification for fusion welding for aerospace applications stipulates a maximum underfill depth of $0.07T$ (where T is the thickness or 3.2 mm in the present work) for Class A welds. Hence, over the range of welding conditions examined,

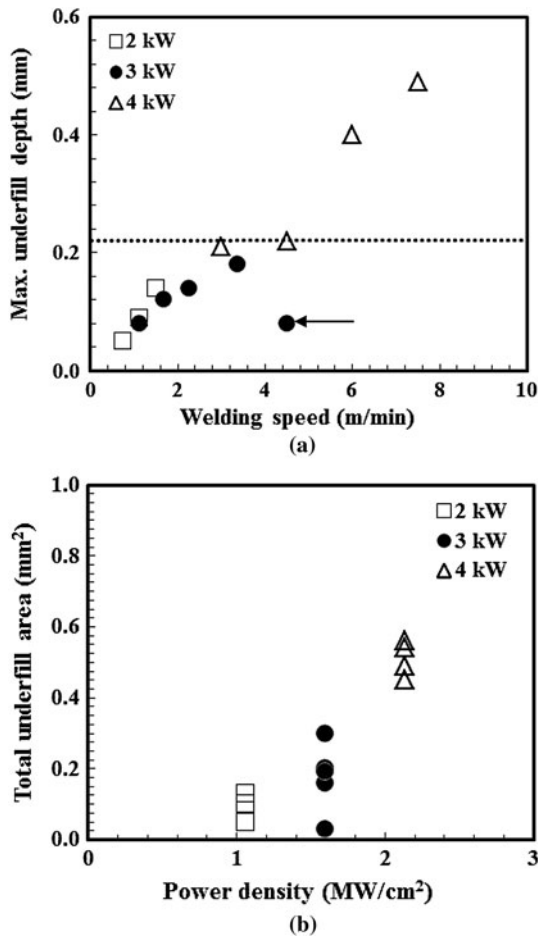


Fig. 4—Effect of (a) welding speed and (b) the power density on the underfill dimensions (the arrow identifies the weld with a LOP that was then welded from both sides).

the Ti-6Al-4V laser welds satisfy Class A requirements if the underfill discontinuity is below 0.22 mm, as indicated by the dashed line in Figure 4(a). At laser powers of 2 and 3 kW, all the welds remained within the acceptable specification. However, at a laser power of 4 kW, the maximum underfill depth just meets the acceptable threshold at the lower welding speeds (higher heat inputs); with increasing welding speed (decreasing heat input) the maximum underfill depth rapidly increases to more than twice the acceptable threshold value. For each laser power level, the maximum underfill depth increases linearly with increasing welding speed for all fully penetrated joints (Figure 4(a)).

As the formation of underfill defects is mainly due to the evaporation and expulsion of molten materials,^[28] the total underfill area increases with increasing laser power density, as shown in Figure 4(b). Specifically, as the laser power density increases, the total vaporization losses increase significantly.^[29,30] At higher heat input (*i.e.* higher laser power or lower welding speed), the extent of evaporation is greater.^[31] If the weld pool temperature is very high, then the escaping vapor may exert a large recoil force on the weld pool surface. When the vapor recoil force exceeds the surface tension force

of the liquid metal at the periphery of the weld pool, liquid metal expulsion or ejection can occur.^[29,30] The higher vapor pressure will cause greater expulsion of the liquid metal,^[32] which will eject at an increasing velocity with increasing laser power density. Both the size of the liquid droplets and size distributions of the expelled particles have been reported to increase with increasing power density.^[29,30]

As a higher welding speed allows lesser interaction time between the laser beam and the workpiece material, the weld pool temperature and recoil force pressure should be lower, and, therefore, the material losses from evaporation and expulsion are also lower. However, as illustrated in Figure 4(a), the maximum underfill depth increases linearly with increasing welding speed for all fully penetrated welds; this suggests that the higher cooling rates associated with the higher welding speeds play a vital role in the formation of the underfill defects. This is probably related to the flow of the molten metal. In particular, at higher welding speeds and the associated faster cooling rates, the molten metal has a shorter time to solidify and fill the surface grooves/cavities.^[28] Thus, the extremely large underfill depths, as observed at the high laser power of 4 kW and high welding speeds of 6.0 to 7.5 m/min, are due to the combined effects of (i) failure to fill the surface grooves at the high cooling rate conditions and (ii) significant evaporation and ejection of the liquid metal at the high laser power densities. These underfill defects can reduce the thickness and thus the load-bearing capacity of the weld region, thereby causing significant stress or strain concentration and favoring the initiation of cracks, which can heavily degrade the mechanical properties.^[17] The influence of these underfill defects on the mechanical performance of the Ti-6Al-4V laser welds will be discussed in greater detail in the section on the tensile properties.

In addition to the two main defects, underfill and porosity, as discussed above, overlap defects were also observed, but only at the high laser power of 4 kW, as shown in Figures 1 and 5. This is due to the occurrence of high recoil force pressures at the high laser power densities. The overlap defects also lead to the formation of a lack of bonding (LOB) between the overlapped liquid metal and the relatively cold workpiece surface. This defect can work as a stress concentrator in the welded joints and thus should be avoided during manufacturing. Notwithstanding its prospective for low heat inputs and high welding speeds, a laser power of 4 kW is a non-conductive parametric condition for laser welding of 3.2-mm thick Ti-6Al-4V as it results in overlap and unacceptable underfill defects.

C. Micro-indentation Hardness and Microstructural Evolution

Figure 6 shows the typical hardness profiles measured at the top, middle, and root regions of a welded joint assembled at 3 kW and 1.69 m/min. For each weld, the lowest and highest hardness values occurred in the BM and FZ, respectively. The average hardness in the BM

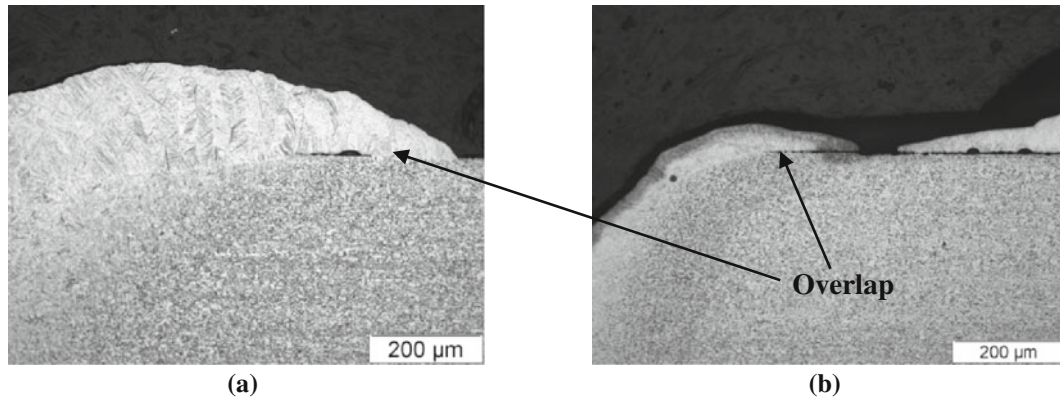


Fig. 5—Typical overlap and lack of bonding (a) 4 kW, 3.0 m/min, and (b) 4 kW, 6.0 m/min.

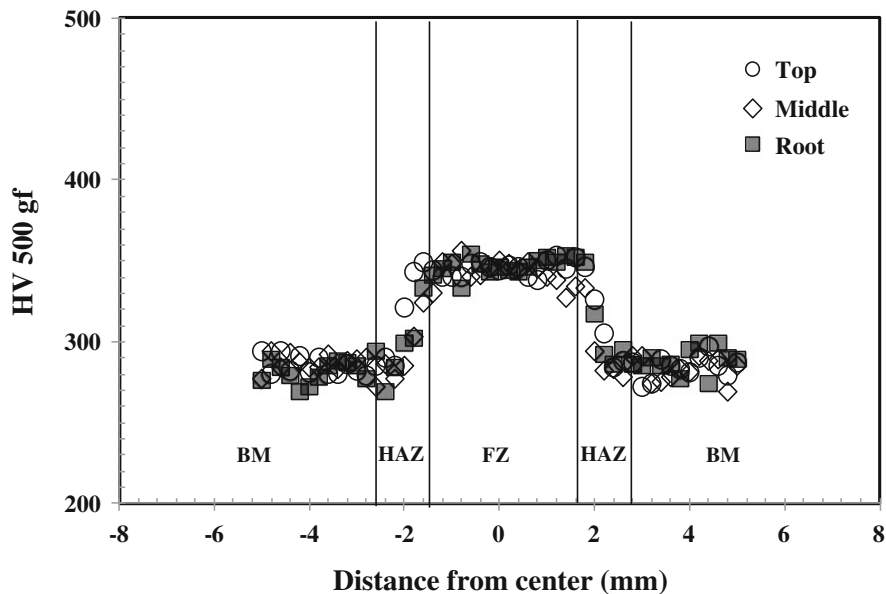


Fig. 6—Typical hardness distribution obtained for the Ti-6Al-4V laser weld assembled at 3 kW and 1.69 m/min.

was 312 ± 8 HV. In the FZ of the weld assembled at a laser power of 3 kW and a welding speed of 1.69 m/min, the average hardness was 360 ± 4 HV, roughly 15 pct greater. The hardness evolution across the weldment can be related to the transformation of the microstructural constituents, namely the α and β phases in Ti-6Al-4V, which have transpired due to the thermal history imparted by the laser welding process, as shown in Figure 7. Specifically, the as-received microstructure of the mill annealed Grade 5 Ti-6Al-4V consisted of equiaxed α with intergranular β , as revealed in Figure 7(a). During laser welding, the temperature in the FZ exceeds the liquidus temperature of Ti-6Al-4V. As such, the FZ macrostructure of the Ti-6Al-4V laser welds (Figure 1) consisted of columnar prior- β grains that epitaxially grow in a direction opposite to that of the heat flow,^[17] *i.e.* from the semi-melted β grains adjacent to the fusion boundary towards the weld centerline where impingement occurs upon solidification. Within the prior- β grains, the microstructure of the

FZ appeared to consist of both diffusionless and diffusional transformation structures. Specifically, the acicular microstructure in FZ (Figure 7(e)) appears to predominately consist of martensite (α'), a supersaturated non-equilibrium hexagonal α phase produced from the diffusionless transformation of the high temperature β phase^[1,33] during rapid cooling associated with laser welding. It is noteworthy that as vanadium suppresses the start of the α' transformation to below ambient temperature, the microstructure in the FZ may also contain evidence of remnant β .^[1] It has been reported that cooling rates in excess of 683 K/s (410 °C/s) are typically needed for the β phase of Ti-6Al-4V to fully transform to α' .^[34] Though the high self-quench rate associated with the laser welding process indubitably promotes diffusionless transformation of the β phase to α' , the presence of α along some of the prior- β grain boundaries (Figure 7(f)) indicates that the cooling rate is close to the lower limit of the cooling rate for α' formation, *i.e.*, 683 K/s (410 °C/s). Previously, for laser

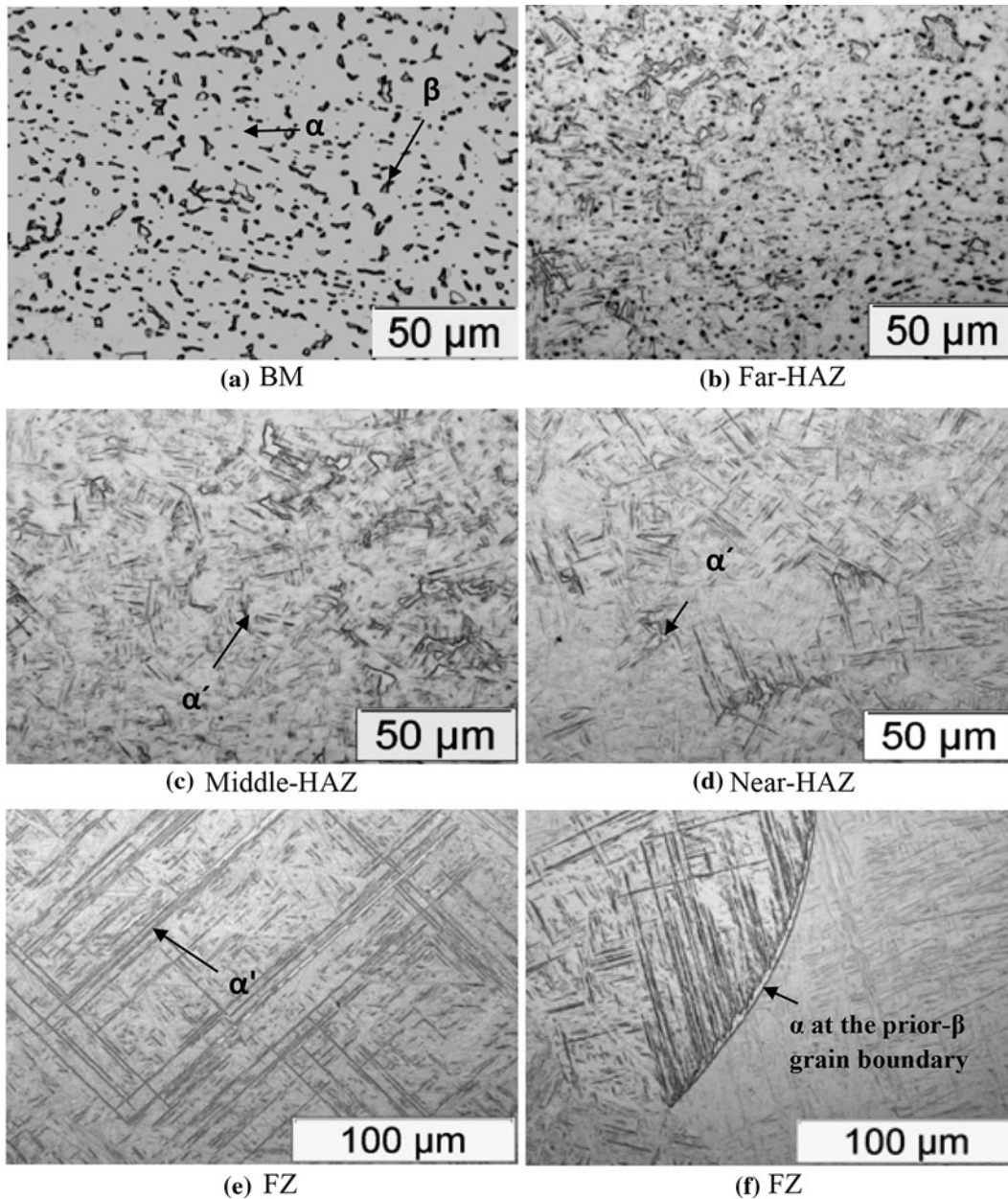


Fig. 7—Typical microstructures in the BM, HAZ, and FZ.

welded Ti-6Al-4V, Akman *et al.*^[4] also associated the increase in the FZ hardness (similar to that observed in the present work) to the formation of α' as a result of the high cooling rates, which supports the findings and observations in the present work.

As evident in Ti-6Al-4V laser welds illustrated in Figure 1, a HAZ between the FZ and the BM exists and is usually sub-divided, on the basis of the β transus temperature [~ 1268 K (995 °C)], into two regions, the near-HAZ and far-HAZ. In the near-HAZ (the region close to the FZ), the thermal conditions during laser welding result in temperatures that surpass the β -transus but remain below the liquidus [~ 1933 K (1660 °C)]; in the far-HAZ (the region close to the BM), the temperature is below the β -transus but above a minimum

temperature required to sufficiently change the microstructure, which depends on transformation kinetics.^[38]

Figures 7(b) through (d) show the typical microstructures in different regions in the HAZ of a welded sample. Similar to the FZ microstructure, the near-HAZ experiences transformation of the β phase to predominately α' (Figure 7(d)); the limited fraction of remnant primary α in the microstructure may be due to the incomplete transformation kinetics during rapid laser heating. Unsurprisingly, the hardness in the near-HAZ was similar to that in the FZ (*e.g.*, 358 ± 9 HV for the welding condition of 3 kW and 1.69 m/min). On the other hand, as revealed in Figures 7(b) through (c), the far-HAZ microstructure consisted of increasing amounts of primary α and intergranular β , concomi-

tantly with a decreasing fraction of α' . Specifically, traversing from the near-HAZ to the BM, the fraction of α' in the microstructure decreases rapidly from nearly 100 pct to zero and, as a consequence, a sharp decrease in hardness transpires in this region.

Figure 8 shows the effect of welding speed and laser power on the average hardness in the FZ, which is reported as a percentage as it was normalized against the

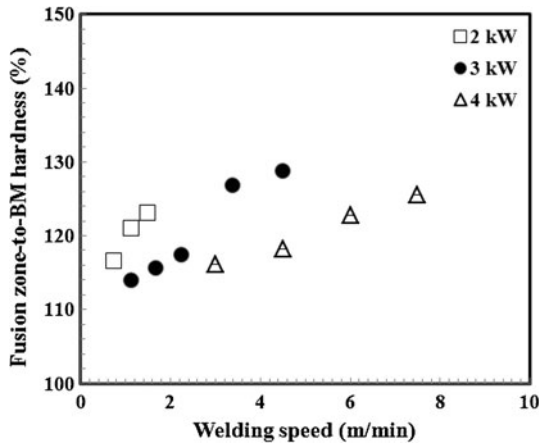


Fig. 8—Effect of the laser processing parameters on the ratio of the average hardness in FZ to that in the BM (in percent).

BM average value of 312 HV. In particular, the average hardness of the FZ was observed to increase with increasing welding speed (*i.e.*, decreasing heat input), which is similar to that observed by Sun *et al.*^[35] At a given welding speed, the average hardness in the FZ decreases with increasing laser power. The evolution in the FZ hardness with welding speed and laser power can be reasoned on the basis of the heat input and its resulting influence on the microstructure. At a constant laser power, increasing the welding speed decreases the heat input and thus increases the cooling rate over the solidification temperature range; likewise, at a constant welding speed, increasing the laser power increases the heat input and thus decreases the cooling rate. Hence holding one of the two parameters constant, at a lower welding speed or higher laser power the prior- β grains are larger in size (Figure 1), and the β transformation microstructures may have a greater fraction of diffusional constituents such as Widmanstätten and grain boundary α . Thus, increasing the welding speed or decreasing the laser power progressively refines the prior- β grain structure (Figure 1) and, the high cooling rate during solidification, promotes diffusionless transformation of the β phase to α' ,^[35] such that the end result is manifested through an increase in the FZ hardness. Nonetheless, it is expected that refinement of the prior- β grain structure should permit maintaining the weld ductility, as it is well known that there is a

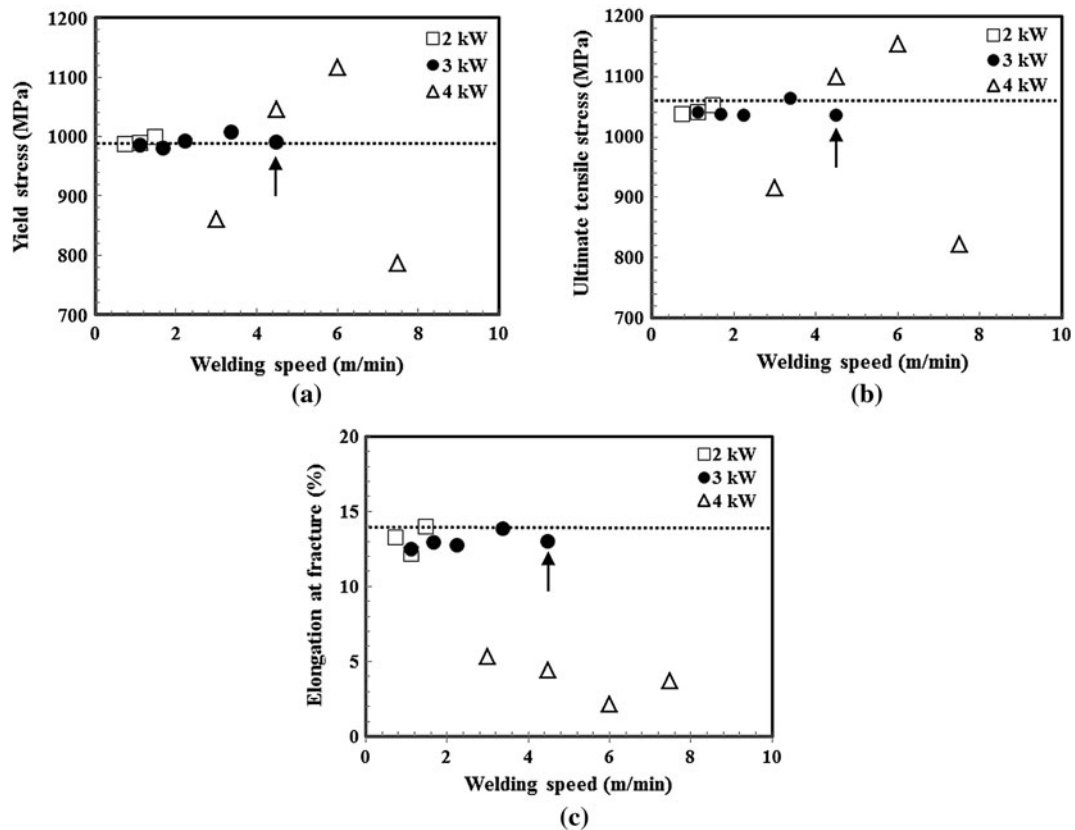


Fig. 9—Global tensile properties of the laser welds (the dashed lines indicate the BM values; the arrow identifies the joint welded from both sides).

propensity for crack propagation along the prior- β grain boundaries.^[6]

D. Global Tensile Properties

Figure 9 shows the influence of the laser power and welding speed on the average global tensile properties that were determined using conventional tensile testing and, for some process conditions (*i.e.* 2 and 3 kW), with DIC. The global tensile properties obtained from both testing methods were quite similar, indicating that the DIC technique is a reliable approach for determining the tensile properties. The welds manufactured using a laser power of 4 kW displayed considerable variations in the yield and ultimate tensile strength (UTS) values, and a significant loss in the elongation, as compared to the BM properties. This loss in ductility may be attributed mainly to the welding defects, especially the underfill, porosity, and overlap (as described earlier), in the welds produced at 4 kW. Significant degradation in the weld ductility is a common issue in the welding of titanium alloys. In contrast, the global tensile properties obtained at 2 and 3 kW were nearly constant over the range of welding speeds employed and similar in value to that of the BM, which had a yield strength (YS) of 996 MPa, an UTS of 1062 MPa and an elongation (El.) of 14 pct. Hence at the low (2 kW) and intermediate (3 kW) laser powers the joint efficiency was nearly 100 pct and no significant loss in weld ductility was apparent within the operational window in the present work. To this end, a significant finding in the present work is that for laser welding of Ti-6Al-4V, targeting a minimal heat input does not necessarily ensure weld quality and performance. In particular, according to the conventional welding practice, a low heat input is generally recommended on the basis of minimizing damage to the assembly that can result from the thermal changes during fusion welding, such as phase transformations, grain coarsening, residual stresses, and distortion.^[36] However, the present findings show clearly that if a low heat input is the main criterion selected for laser welding of Ti-6Al-4V (*i.e.* at 4 kW), the resulting defects (underfill, porosity, and overlap) override any

possible gains from reducing the thermal damage to the assembly. Hence, though the operational process window is relatively large for manufacturing high performance Ti-6Al-4V laser welds, the combination of the laser power and welding speed must be judiciously selected to ensure that the weld bead characteristics

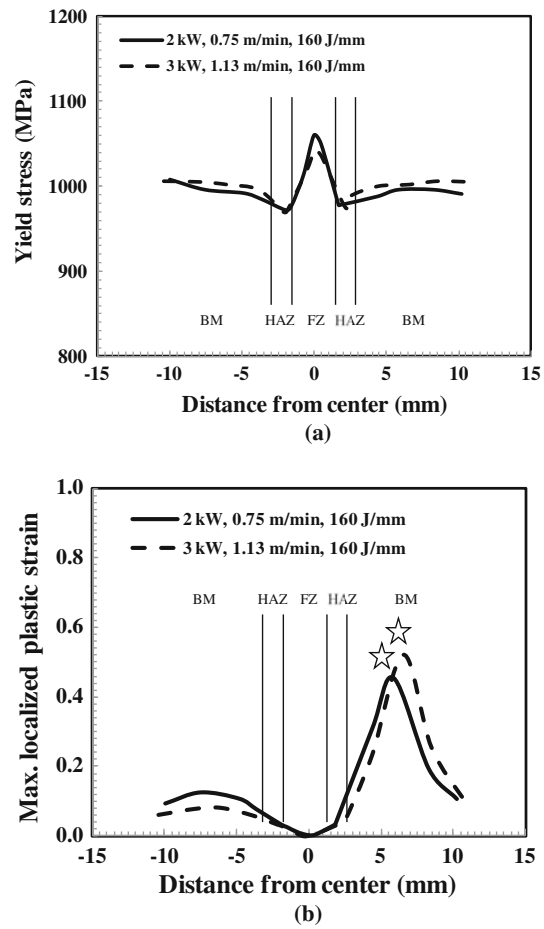


Fig. 11—Typical distributions of the local tensile properties at a heat input of 160 J/mm.

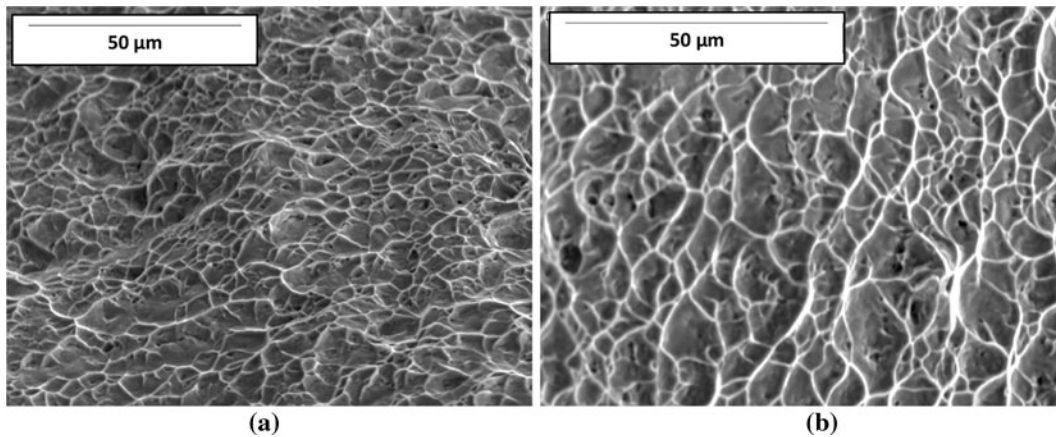


Fig. 10—SEM images of the tensile fracture surfaces from welds assembled at (a) 2 kW, 0.75 m/min, 160 J/mm, and (b) 3 kW, 1.13 m/min, 160 J/mm, both of which exhibited failure in the BM.

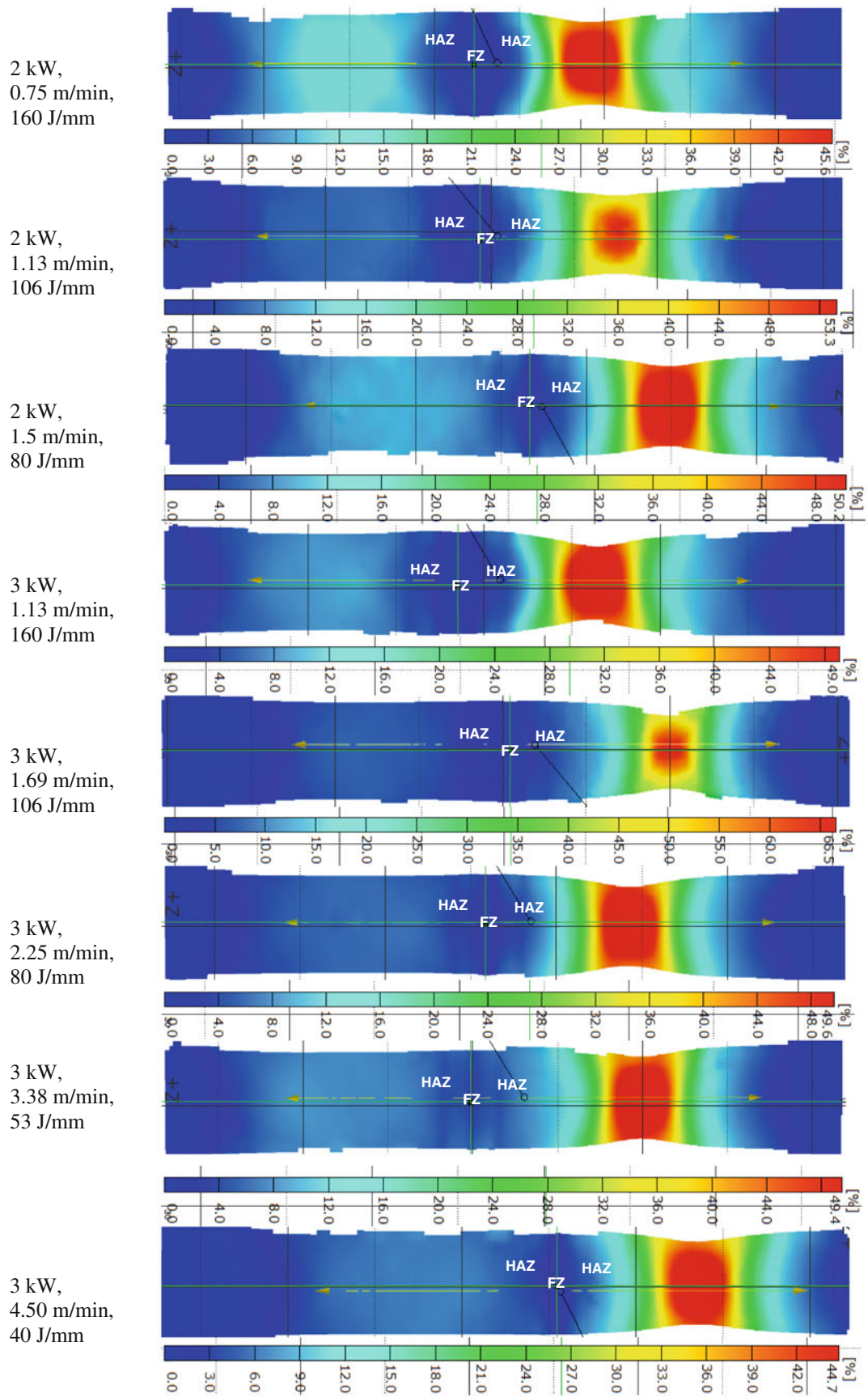


Fig. 12—Strain maps just before rupture of the tensile samples.

exhibit minimum levels of welding defects such as underfill and porosity. In the case of 3.2-mm-thick Ti-6Al-4V, low (2 kW) and intermediate (3 kW) laser powers with the fastest welding speed that can allow complete penetration appear to result in the high mechanical performance with no loss in both strength and ductility, as illustrated in Figure 9.

As shown in Table I, failure of all the welds manufactured at 2 and 3 kW occurred in the BM, while the welds joined at 4 kW failed in either the HAZ or FZ. It is interesting to note that this behavior in the tensile failure for the 3.2-mm-thick welds, as obtained in the present work, is consistent with earlier results on 5.1-mm-thick Ti-6Al-4V laser welds.^[8] In particular, tensile failure is predominantly triggered by the main welding defects, such as underfill and porosity. The initiation of cracking is controlled by the underfill defect while its propagation is determined by the porosity level. Cracks usually form at the underfill defect if its depth exceeds the threshold value, which is approximately 6 pct of the workpiece thickness. The cracks can then propagate through the FZ at a high level of porosity, or through the HAZ at a low level of porosity. If both the underfill depth and porosity level are low, the weld region comprising the FZ and HAZ appears to be stronger than the BM and thus failure usually appears in the latter.^[8] This can be substantiated for the 3.2-mm-thick Ti-6Al-4V welds manufac-

tured at 2 and 3 kW, which exhibited tensile failure in the BM and had underfill depth values (0.04 to 0.19 mm) that were lower than the threshold (Figure 4(a)). Failure in BM for these welds can be reasoned on the basis of a high weld integrity (small underfill depth and low porosity) and a strong FZ (e.g., high hardness) microstructure (α'). The typical tensile fracture surfaces, as shown in Figure 10, reveal cup and cone shape configurations with copious dimples or microvoids, which are indicative of ductile failure. It is also noteworthy that the appearance of some pores in FZ especially for the 2 kW welds does not lead to any degradation in the global tensile properties, including ductility, and may be attributed to the low porosity level (less than 1 pct of the FZ area) and the relatively round shape of the pores. In contrast, for the welds manufactured at a laser power of 4 kW, the underfill depth was at or above the threshold value of 0.22 mm and, for some welds, the porosity in the FZ (Figure 3) was also relatively high (e.g. 0.5 pct). Hence, the effect of the strong FZ microstructure (α') is overridden by the welding defects that control the fracture during tensile loading. This present study also reinforces the use of a lower maximum tolerable underfill depth of about 6 pct of the workpiece thickness, which is slightly stricter than the existing 7 pct threshold according to the aerospace specification for fusion welding (AWS D17.1).^[27]

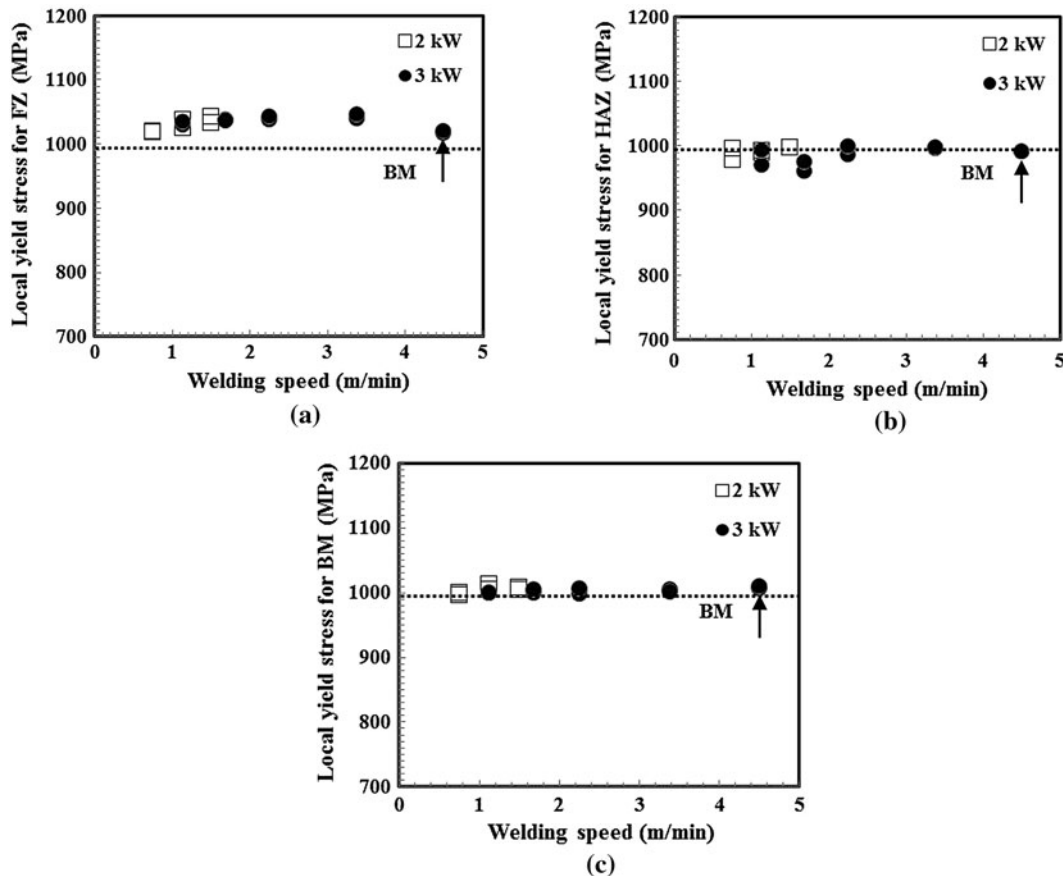


Fig. 13—Yield stress values in the different regions of the welds assembled at laser powers of 2 and 3 kW (the arrow identifies the results obtained from a joint that was welded from both sides).

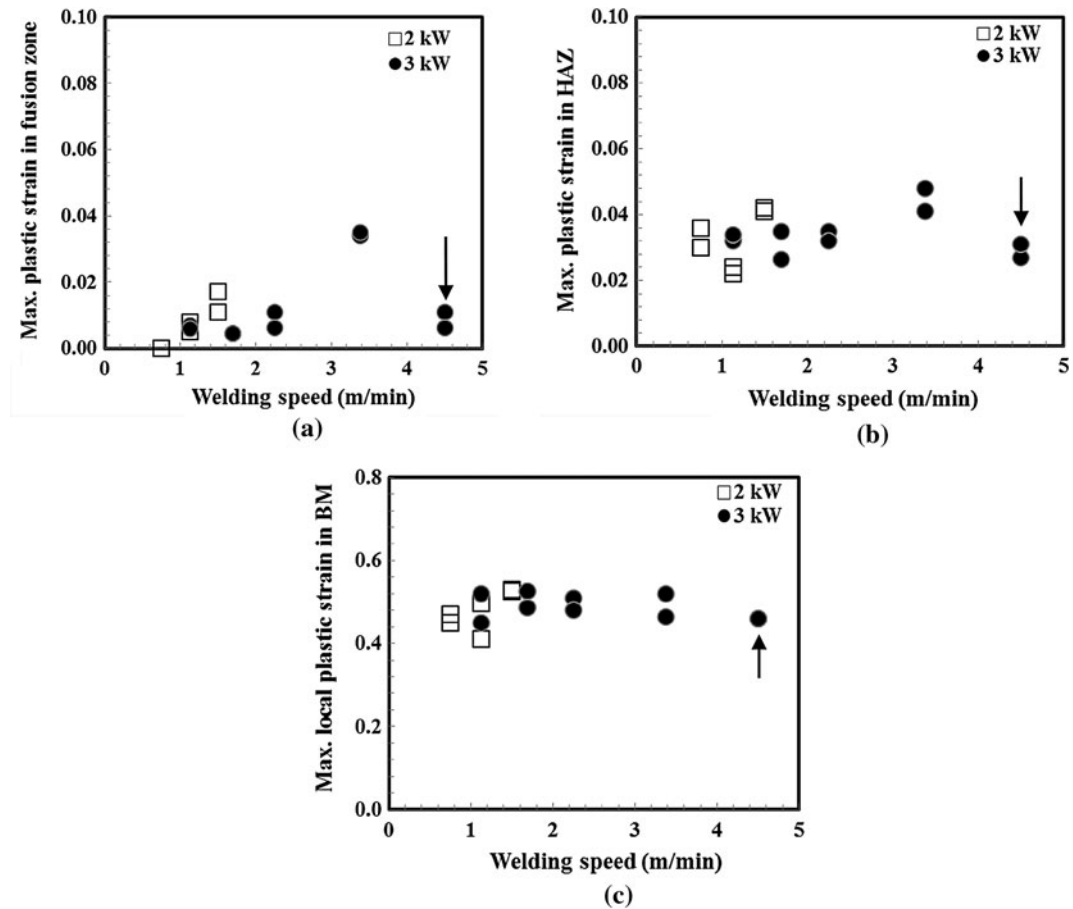


Fig. 14—Maximum local plastic strain experienced in different regions of the welds assembled at 2 and 3 kW during tensile testing (the arrow identifies the results obtained from a joint that was welded from both sides).

Having characterized the tensile properties of the as-received BM (YS of 996 MPa, UTS of 1062 MPa, and El. of 14 pct), the joint efficiency, ratio between UTS of the welded joint to that of BM could be determined. For welds assembled at 3 kW of laser power, the average joint efficiency was calculated to be 98.2 pct and ranged from 97.5 to 100 pct. In contrast, the joint efficiency for the welds manufactured at a laser power of 4 kW varied from 77.5 to 108.5 pct and highlights the importance of the welding defects on the mechanical performance of the joints.

E. Local Tensile Properties

Figure 11 shows the representative profiles of the local tensile properties along the gauge length for weldments assembled at 160 J/mm. Compared to the BM, the yield stress is higher in the FZ but slightly lower in the HAZ. This finding is consistent with the reported results on Ti-6Al-4V of a reduced strength for a microstructure quenched from a temperature of 1073 K (800 °C).^[37] Figure 12 shows the strain distribution along the gauge length of the tensile sample just before rupture. For each strain distribution, the adjacent gradients in color (or shaded) indicate the relative intensity. Hence, in these strain maps, the region of

strain concentration, indicated as the area with the highest intensity, corresponds to the location of the fracture that occurred immediately afterward. Using the Aramis strain distribution maps, the strain localization just prior to rupture can be methodically examined. As indicated in Figures 11(b) and 12, the maximum local strain is concentrated within the BM for all the welds assembled at 2 and 3 kW. Hence despite the presence of some underfill and porosity defects, strain localization in the FZ is minimal and may be attributed to the local strengthening effect of the α' microstructure. Thus, it can be concluded that the strengthening effect of the FZ microstructure can compensate for the weakening effect of the welding defects, such as underfill and porosity, as long as the size/amount of these remain below the recommended threshold/critical values.

Figures 13 and 14 show the variation in the local tensile properties as a function of the welding speed at laser powers of 2 and 3 kW. It is apparent that the yield stress values in the FZ are unequivocally higher than that of the BM and increase slightly with increasing welding speed for the fully penetrated single pass welds. This is attributed to the finer prior- β grain structure and, in turn, more refined α' structure^[38] associated with the increased welding speed. Similarly, the maximum plastic strain in the FZ, just before fracture (Figure 14(a)), also

increases with increasing welding speed. In contrast, the yield stress in the HAZ (Figure 13(b)) is nearly the same as that of the BM. The yield stress in the region of the BM (Figure 13(c)) of the welds remains relatively constant and is the same as that obtained for the unwelded material using conventional tensile testing (996 MPa), which corroborates the reliability of the DIC technique for determining the local tensile properties. As remarked from Figure 14, the local plastic strains in the BM (40 to 55 pct) and HAZ (2 to 5 pct) were greater than those in FZ (typically under 2 pct) that reflected the inherent characteristics of the microstructure, *i.e.*, α' in the FZ would exhibit a higher resistance to deformation than the mixed structure (α' , Widmanstätten, α and β) in the HAZ and, in turn, the $\alpha + \beta$ structure in the BM. These local strain values in the BM and HAZ are in contrast to the global/average strain value, which was about 14 pct, as indicated in Figure 9(c).

IV. CONCLUSIONS

1. The weld integrity is mainly determined by the underfill depth and porosity, but the former is much more damaging and thus it is recommended that the maximum tolerable underfill depth should not exceed 6 pct of the workpiece thickness, which is slightly stricter than the existing threshold of 7 pct according to the present aerospace specification for fusion welding (AWS D17.1).
2. At a high laser power (4 kW) and high laser power density, significant defects, such as underfill, porosity, overlap, and associated LOB, occurred and caused marked variations in tensile properties along with degradation in weld ductility due to premature failure in either the FZ or the HAZ.
3. A wide range of heat inputs can be used during laser welding to fully penetrate the Ti-6Al-4V butt joints through reasonable combinations of the laser power and welding speed. However, intermediate to high levels of heat input, obtained at the low and intermediate laser power (2 and 3 kW) render high weld integrity due to the reduced underfill depth. The common practice of targeting a low heat input is thus not recommended for laser welding of Ti-6Al-4V.
4. Compared with the BM, a higher hardness is obtained in the FZ due to the formation of the martensite. The hardness in the HAZ gradually decreases from the near-HAZ to the far-HAZ due to the gradual drop in the martensite content. The average hardness in the FZ was observed to increase with increasing welding speed or decreasing laser power.
5. Within the acceptable limit for the maximum underfill depth (*i.e.*, less than 6 pct of the workpiece thickness), the global tensile properties of the Ti-6Al-4V laser welds are similar to those of the BM and remain nearly constant over a wide range of welding speeds or heat inputs. Therefore, no loss and/or degradation in both the tensile strength and

weld ductility occur within this process operating window. The absence of a ductility loss in the laser welds is a great advantage of using a high energy density process over conventional arc welding.

6. Both the higher hardness and local yield stress values in the FZ are attributed to the formation of martensite that inherently enables local strengthening at the expense of ductility. In contrast, the HAZ is very slightly weakened (nearly similar to or slightly lower yield strength) as compared to the BM. The YS in the FZ also increased slightly with increasing welding speed, while that in the HAZ remained nearly constant over the welding speeds applied for the fully penetrated single pass laser welds.

ACKNOWLEDGMENTS

The technical support of E. Poirier, X. Pelletier, and D. Chiriac during laser welding, metallographic preparation, and tensile testing using ARAMIS, respectively, are highly acknowledged.

REFERENCES

1. M.J. Donachie: *Titanium: A Technical Guide*, ASM International, Materials Park, OH, 1989.
2. J.L. Barreda, F. Santamaria, X. Azpiroz, A.M. Irisarri, and J.M. Varona: *Vacuum*, 2001, vol. 62, pp. 143–50.
3. Q. Yunlian, D. Ju, H. Quan, and Z. Liying: *Mater. Sci. Eng. A*, 2000, vol. 280, pp. 177–81.
4. E. Akman, A. Demir, T. Canel, and T. Sinmazçelik: *J. Mater. Process. Technol.*, 2009, vol. 209, pp. 3705–13.
5. A.H. Kazaz, M. Medraj, X. Cao, M. Jahazi, and M. Xiao: in *44th Annual Conference of Metallurgist of CIM*, Calgary, AL, J.P. Martin, ed., 2005, pp. 137–49.
6. D.L. Olson, T.A. Siewert, S. Liu, and G.R. Edwards: *ASM Handbook, Welding, Brazing, and Soldering*, ASM International, Materials Park, OH, 1993.
7. A. Costa, R. Miranda, L. Quintino, and D. Yapp: *Mater. Manuf. Process.*, 2007, vol. 22, pp. 798–803.
8. A.S.H. Kabir, X. Cao, J.G. Baradari, P. Wanjara, J. Cuddy, A. Birur, and M. Medraj: *Adv. Mater. Res.*, 2012, vol. 400, pp. 857–62.
9. A.S.H. Kabir, X. Cao, P. Wanjara, J. Cuddy, A. Birur, and M. Medraj: *Can. Metall. Q.*, 2012, vol. 51, pp. 320–27.
10. A.S.H. Kabir, X. Cao, P. Wanjara, J. Gholipour, J. Cuddy, A. Birur, and M. Medraj: in *MS&T2010: Laser Applications in Materials Processing*, 17–21 October 2010, Houston, TX, S. Copley, J. Schneider, and A. Black, eds., 2010, pp. 2787–97.
11. A. Kabir, X. Cao, J. Gholipour, P. Wanjara, J. Cuddy, A. Birur, and M. Medraj: *Metall. Mater. Trans. A*, 2012, vol. 43A, pp. 4171–84.
12. W.D. Lockwood and A.P. Reynolds: *Mater. Sci. Eng. A*, 2003, vol. 339, pp. 35–42.
13. W.D. Lockwood, B. Tomaz, and A.P. Reynolds: *Mater. Sci. Eng. A*, 2002, vol. 323, pp. 348–53.
14. B. Boyce, P. Reu, and C. Robino: *Metall. Mater. Trans. A*, 2006, vol. 37A, pp. 2481–92.
15. ASTM: *Standard Test Methods for Tension Testing of Metallic Materials E 8M-04*, American Society for Testing and Materials, Materials Park, OH, 2004.
16. P. Rastogi, M. Sutton, S. McNeill, J. Helm, and Y. Chao: *Photomechanics*, Springer, Berlin/Heidelberg, 2000, pp. 323–72.
17. X. Cao, G. Debaecker, E. Poirier, S. Marya, J. Cuddy, A. Birur, and P. Wanjara: *J. Laser Appl.*, 2011, vol. 23, p. 012004.
18. C. Dawes: *Laser Welding*, McGraw-Hill, New York, NY, 1992.

19. X. Cao, M. Jahazi, J.P. Immarigeon, and W. Wallace: *J. Mater. Process. Technol.*, 2006, vol. 171, pp. 188–204.
20. Z. Khaled: *J. Mater. Eng. Perform.*, 1994, vol. 3, pp. 419–34.
21. D.R. Mitchell: *Weld. J.*, 1982, vol. 61, pp. 157s–67s.
22. F. Karimzadeh, M. Salehi, A. Saatchi, and M. Meratian: *Mater. Manuf. Process.*, 2005, vol. 20, pp. 205–19.
23. G. Lutjering and J.C. Williams: *Titanium*, 2nd ed., Springer, Berlin, 2007.
24. M. Pastor, H. Zhao, and T. DebRoy: *Rev. Metall.*, 2000, vol. 36, pp. 108–17.
25. T. Mohandas, D. Banerjee, and V. Kutumba Rao: *Metall. Mater. Trans. A*, 1999, vol. 30A, pp. 789–98.
26. A. Matsunawa, J.-D. Kim, N. Seto, M. Mizutani, and S. Katayama: *J. Laser Appl.*, 1998, vol. 10, pp. 247–54.
27. AWS: *Specification for Fusion Welding for Aerospace Application, D17.1*, American Welding Society, Miami, OH, 2001.
28. M. Pastor, H. Zhao, R.P. Martukanitz, and T. DebRoy: *Weld. J.*, 1999, vol. 78, pp. 207s–16s.
29. X. He, T. DebRoy, and P.W. Fuerschbach: *J. Phys. D*, 2003, vol. 36, p. 3079.
30. X. He, J.T. Norris, P.W. Fuerschbach, and T. DebRoy: *J. Phys. D*, 2006, vol. 39, p. 525.
31. X. Cao and M. Jahazi: *Opt. Lasers Eng.*, 2009, vol. 47, pp. 1231–41.
32. J. Weston, A. Jones, and R. Wallach: *Proceedings of the 6th International Conference on Welding and Melting by Electron and Laser Beams*, Toulon, France, 1998, p. 187.
33. A.B. Short: *Mater. Sci. Technol.*, 2009, vol. 25, pp. 309–24.
34. T. Ahmed and H.J. Rack: *Mater. Sci. Eng. A*, 1998, vol. 243, pp. 206–11.
35. Z. Sun, D. Pan, and W. Zhang: *Sixth International Conference on Trends in Welding Research*, Pine Mountain, Georgia, USA, 2002, pp. 760–67.
36. G.A. Knorovsky, P.W. Fuerschbach, S.E. Gianoulakis, and S.N. Burchett: in *Trends in Welding Research: Proceedings of the 4th International Conference*, 5–9 June 1995, Gatlinburg, TN, H.B. Smartt, J.A. Johnson, and S.A. David, eds., 1995, pp. 479–86.
37. Y. Lee, M. Peters, and G. Welsch: *Metall. Trans. A*, 1991, vol. 22A, pp. 709–14.
38. P. Wanjara, M. Brochu, and M. Jahazi: *Mater. Manuf. Process.*, 2006, vol. 21, pp. 439–51.